Rare Metal Materials and Engineering
Volume 48, Issue 2, February 2019
Available online at www.rmme.ac.cn

Science Press

Cite this article as: Rare Metal Materials and Engineering, 2019, 48(2): 0433-0439.

ARTICLE

Effects of Stress Triaxiality and Lode Parameter on Ductile Fracture in Aluminum Alloy

Liu Lixi[1,2], Zheng Qingli[1], Zhu Jian[3], Li Zhiqiang[1,3,4]

[1] Taiyuan University of Technology, Taiyuan 030024, China; [2] Xi'an Jiaotong University, Xi'an 710049, China; [3] Shanxi Key Laboratory of Material Strength & Structural Impact, Taiyuan 030024, China; [4] State Key Laboratory of Explosion Science and Technology, Beijing Institute of Technology, Beijing 100081, China

Abstract: Many theoretical and experimental studies showed that stress triaxiality has an important influence on ductile fracture. However, recent studies showed that Lode parameter, which can be linked to normalized third stress invariant, is also an essential factor. In the present study, round notched bar and flat grooved plate specimens made of 7075 aluminum alloy were used to assess the effect of stress triaxiality and Lode parameter on ductile fracture and on the corresponding microscopic mechanism. Quasi-static tensile tests and parallel numerical simulations were conducted to obtain stress triaxiality, Lode parameter and failure locus. A fractographic analysis was performed to determine the rules of void evolution under different stress states. The results show that stress triaxiality and Lode parameter have an important influence on failure strain. The effect of Lode parameter decreases with the increase in stress triaxiality. The fractographs show that the size of the void decreases with the increase of stress triaxiality, and the morphologies of the voids of different Lode parameters are obviously different. The nucleation rate and growth degree of secondary voids are also affected by Lode parameter.

Key words: stress triaxiality; failure strain; Lode parameter; fractography

In recent years, the development of automobile industry has resulted in a rapid growth in the number of vehicles, which has caused a series of problems, such as traffic accident, lack of resources, and environmental pollution[1]. Therefore, particular attention must be paid to safety, energy saving and environmental protection, and vehicle light-weight[2,3] is an important factor. Demands on passive safety, fuel efficiency, and emission reduction are leading car designers to consider substantial weight reduction. One way to achieve lightweight design with good crashworthiness is to use new light materials such as aluminum alloy, magnesium alloy and composite. Among these materials, aluminum alloy profiles have become increasingly important in the construction of car body structures because of their advantages, such as light density, high specific strength, specific stiffness, and 50% higher energy absorption than steel during a collision[4,5]. For example, six-series aluminum alloys[6] have already become important lightweight materials in vehicle industry, and seven-series aluminum alloys[7,8] have been used in the design of car bumper and engine rocker arms.

Ductile fracture is a complicated process which is controlled by the microstructure of the material and the stress state during the deformation process. During collisions, material deformation is usually composed of not merely the basic mode, such as compression, tension, and torsion, but a combination of at least two kinds of basic deformation modes[9]. The stress state of each point may also change over time. The fracture mode is different for different materials and different loading histories[10,11]. Hence, a detailed study of fracture is necessary and valuable.

Received date: February 23, 2018
Foundation item: Natural Science Foundation of Shanxi Province (201601D011011); Opening Project of State Key Laboratory of Explosion Science and Technology (KFJJ16-07M); National Natural Science Foundation of China (11672199)
Corresponding author: Li Zhiqiang, Ph. D., Professor, Institute of Applied Mechanics and Biomedical Engineering, Taiyuan University of Technology, Taiyuan 030024, P. R. China, Tel: 0086-351-6014455, E-mail: lizhiqiang@tyut.edu.cn

In recent years, the study of ductile fracture has received more and more attention. Bridgman's experiments showed that hydrostatic stress has some effect on failure of materials and the influence of hydrostatic stress has been embedded in stress triaxiality[12]. Many theoretical and experimental studies showed that stress triaxiality has a significant influence on ductile fracture[13–15]. Failure strains change under different stress triaxialities, and failure locus is not monotonic across the whole range of stress triaxiality[16-18]. As the only fracture parameter, stress triaxiality is generally used to distinguish fracture mechanism. Recently, some researchers have demonstrated that characterizing the stress state using only stress triaxiality is inadequate[19,20]. Another fracture controlling parameter is the third invariant of deviatoric stress tensor (which is related to Lode parameter), and it plays a critical role in providing a better fracture prediction along with the stress triaxiality[21,22].

Therefore, stress triaxiality (η) and Lode parameter (μ_σ) are introduced to measure the stress state of materials, and they are defined, as follows:

$$\eta = \frac{\sigma_{\mathrm{m}}}{\bar{\sigma}} = \frac{1}{3}\frac{I_1}{\sqrt{3J_2}} \tag{1}$$

$$\mu_\sigma = \cos(3\theta) = \frac{3\sqrt{3}}{2}\frac{J_3}{J_2^{3/2}} \tag{2}$$

where σ_{m} is the mean stress, $\bar{\sigma}$ is the von Mises stress, θ is Lode angle that ranges from 0 to π/3. I_1, J_2 and J_3, which represent the first stress invariant, second and third deviatoric stress invariants, respectively, are defined, by

$$I_1 = 3\sigma_{\mathrm{m}} = \sigma_1 + \sigma_2 + \sigma_3 \tag{3}$$

$$J_2 = \frac{1}{6}\left[(\sigma_1-\sigma_2)^2 + (\sigma_1-\sigma_3)^2 + (\sigma_2-\sigma_3)^2\right] \tag{4}$$

$$J_3 = (\sigma_1-\sigma_{\mathrm{m}})(\sigma_2-\sigma_{\mathrm{m}})(\sigma_3-\sigma_{\mathrm{m}}) \tag{5}$$

σ_1, σ_2 and σ_3 denote principal stresses. It is assumed that $\sigma_1 \geq \sigma_2 \geq \sigma_3$.

In addition to macroscopic fracture, stress triaxiality and Lode parameter affect the microscopic mechanism of ductile failure. From a micromechanical point of view, ductile fracture of metals is caused by the nucleation, growth and coalescence of the existing micro-voids. These micro-voids are formed either by debonding or by cracking of second phase particles. If the growth rule of these voids could be grasped, improvement in the resistance of fracture and failure strength could be achieved. So it is valuable to study the mechanical factors controlling the micro-change process of ductile fracture. Several studies demonstrated that stress triaxiality directly affects the growth of voids and determines whether ductile fracture occurs[23-25]. For Lode parameter, it was shown that different values of the Lode parameter can lead to different deformation modes of the voids under constant stress triaxiality[26, 27].

This work aims to determine experimentally the influence of stress triaxiality and Lode parameter on ductile fracture and on the corresponding microscopic mechanism.

1 Experiments and Simulations

1.1 Material, specimens, and experimental setup

The 7075 aluminum alloy was investigated in this study. The seven-series high hardness and strength aluminum alloys have gradually attracted the attention of carmakers because of the advantages of high strength, low density, and high recovery rate. The 7075 aluminum alloy was a typical seven-series aluminum alloy, which belonged to Al-Zn-Mg-Cu hard aluminum alloy. The chemical composition of this material is listed in Table 1. The dimensional data of the specimens are shown in Fig.1. A smooth round bar specimen was used to characterize the elasticplastic behavior of the 7075 aluminum alloy. Round bar specimens of different notch radii R and flat plate specimens of different groove radii r were used to determine the stress-strain behaviors under different stress triaxialities and Lode parameters and to evaluate failure properties. The specimens were sampled and machined in the rolling direction of the plate. The radii of the notches were equal to 2, 3, 4, and 6 mm, and the radii of the grooves were 1.5, 2, 4, and 8 mm. Two specimens were machined for different radii of notches and grooves to ensure that the experiments were correct and repeatable. Tensile tests were conducted using a CMT-5105A universal material test machine. The specimens were held at each end and stretched uniaxially. The tests were performed under quasi-static loading conditions and the tensile velocity was 5 mm/min. Variation in displacement was measured using an extensometer because the displacement of the crosshead was not equal to the displacement of the specimens. The load-displacement responses were recorded using the RG test control system.

The engineering stress-strain curve could be obtained directly by performing the smooth round bar tensile test. The Young's modulus, yield strength, and tensile strength could be easily obtained from the curve. Then, the true stress-strain curve could be drawn using the following formulas:

$$\bar{\sigma} = \sigma(1+\varepsilon) \tag{6}$$

$$\bar{\varepsilon} = \ln(1+\varepsilon) \tag{7}$$

where $\bar{\sigma}$ represents the true stress, σ represents the engineering stress, $\bar{\varepsilon}$ represents the true strain, and ε represents the engineering strain. However, Eqs.(6), (7) were only valid before necking[28]. After the emergence of necking, the cross section of the specimen no longer varied linearly, and the material of the neck was no longer in a simple tension state.

Table 1 Chemical composition of the 7075 aluminum alloy (wt%)

Si	Fe	Cu	Mn	Mg	Cr	Ni	Zn	Ti	Al
0.12	0.27	1.71	0.25	2.66	0.22	0.017	5.86	0.04	Bal.

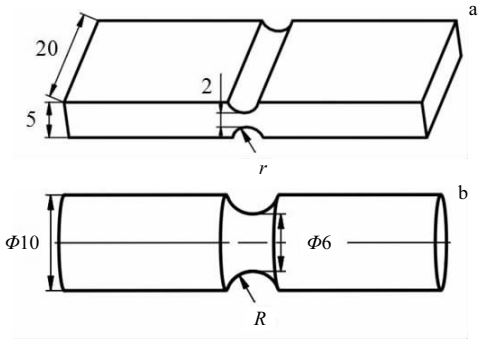

Fig.1 Main dimensional data of two kinds of specimens: (a) flat grooved plate and (b) notched round bar

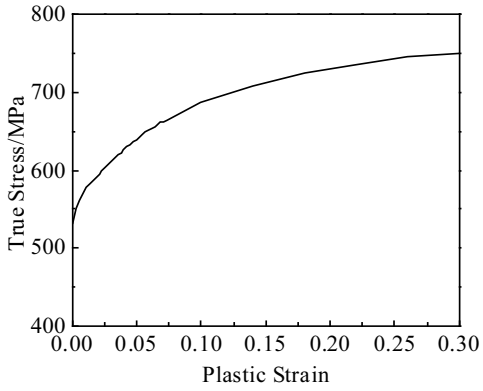

Fig.2 True stress-plastic strain curve of the 7075 aluminum alloy

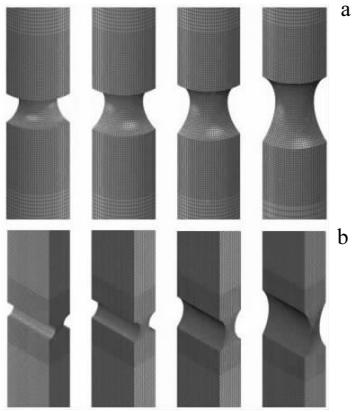

Fig.3 Finite element models of two kinds of specimens: (a) notched round bar models and (b) flat grooved plate models

A trial-and-error method[29] was used to obtain the correct stress-strain relation after necking by modifying the true stress-strain curve. First, the true stress-strain relation obtained by Eqs.(6), (7) was used to simulate the smooth round bar tensile process. Then, the load-displacement curve obtained via the numerical simulation was compared with the experimental result and the true stress-strain curve was modified until no apparent differences existed between the two curves. Multiple attempts should be made to obtain the correct shape after necking. The correct true stress-plastic strain curve of the 7075 aluminum alloy obtained by the aforementioned method is shown in Fig.2.

1.2 Numerical simulation for the round bar specimens

The tensile tests of the round bar specimens were numerically simulated using a commercial finite element (FE) code, namely, ABAQUS/STANDARD, to obtain individual components of the stress and strain tensors at the center region of the notches. According to the size and symmetry of the specimens, their quarter FE models were established with the reduced eight-node solid elements (C3D8R), as shown in Fig.3a.

The mesh was refined at the gauge section of the specimen, and the approximate size of densified grid is 0.25 mm. The 7075 aluminum alloy was modeled using an isotropic hardening plastic constitutive model without strain rate effect. The mechanical parameters of this material are listed in Table 2. Similar to the loading conditions of the tensile test, a constant tensile speed of 5 mm/min was prescribed at one end of the model, whereas the fixed boundary condition was applied to the other end. Symmetry constraints were exerted in two symmetry planes.

The correlations of the deformed shapes between the numerical simulations and experiments are high, as shown in Fig.4. The numerical results accurately simulate the necking effects of the notch regions of the tested specimens. The minimum cross sectional diameters obtained from the fractured specimens are 5.70, 5.66, 5.60, and 5.48 mm, which are very close to 5.74, 5.69, 5.62, and 5.46 mm, respectively, as measured by the numerical simulations. Fig.5 shows the representative load-displacement curves obtained via the numerical simulations and experiments. The FEM responses agree well with the experiments. This finding indicates that the numerical simulation can accurately predict the experimental process.

1.3 Numerical simulation for flat plate specimens

For flat plate specimens, half of each specimen using eight-node solid elements (C3D8R) was modeled in ABAQUS (see Fig.3b). The FE models were built with large elements at the shoulders and small elements at the gauge sections. The loading condition of the flat plate model was the same as that for the round bar model. The changes in shape at the groove region, which occurred in the test, were also successfully captured in the simulation. Fig.6 shows the comparison of the

Table 2 Material properties of 7075 aluminum alloy

Young's modulus/GPa	Yield stress/MPa	Poisson's ratio	Density/ g·cm^{-3}	True stress-plastic strain curve
67	532.51	0.33	2.810	Fig.2

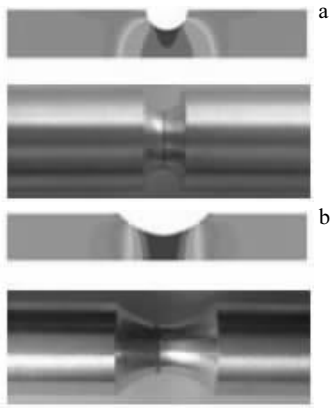

Fig.4 Comparison of the fractured specimen and corresponding FE model: (a) R=2 mm and (b) R=6 mm

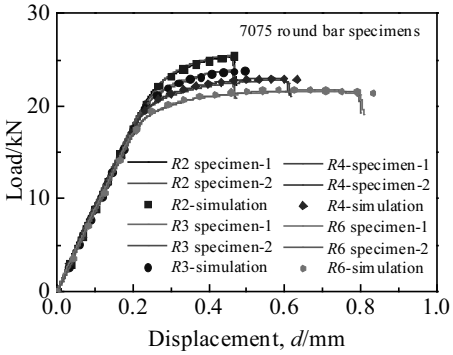

Fig.5 Load-displacement curves for round bar specimens

representative specimen and the corresponding FE model. The numerically-obtained model correlates well with the specimen. The minimum cross sectional width and thickness obtained from the fractured specimen are 17.3 and 1.77 mm, respectively, which are similar to 17.0 and 1.78 mm, as measured via the simulations. Two representative load-displacement curves were obtained via the numerical simulations and the experiments. The curves are shown in Fig.7. The FEM responses also agree well with the responses obtained from the experiments.

2 Effect of Stress Triaxiality and Lode Parameter on Failure Strain

The failure in the tests is defined by a sudden drop of the load-displacement curves. The equivalent plastic strain at the fracture initiation site is regarded as the failure strain and the center of the notch or groove of the FE model is regarded as the fracture initiation site.

According to Eqs.(1~5), stress triaxiality and Lode parameter can be calculated by extracting three principal stresses from the center of the FE model. The curves of the stress triaxiality versus the equivalent plastic strain are obtained for cases with R=4 mm and r=4 mm, as shown in

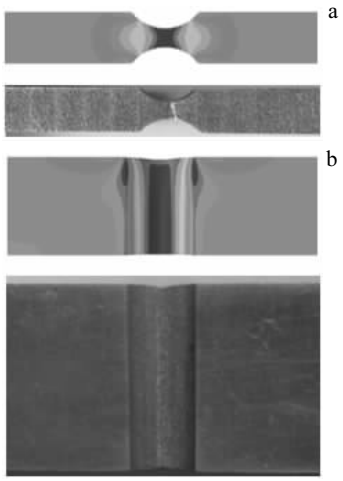

Fig.6 Comparison of the fractured specimen and corresponding FE model: (a) thickness comparison and (b) width comparison

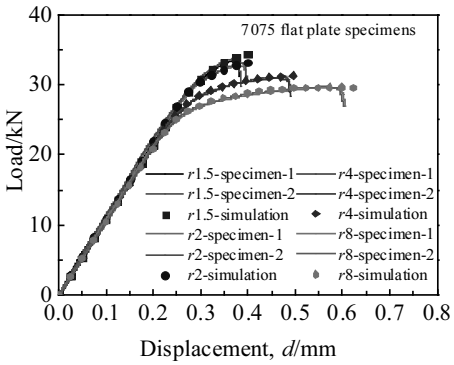

Fig.7 Load-displacement curves for flat plate specimens

Fig.8. It is found that stress triaxialities continue to change with increase in the equivalent plastic strain. This observation indicates that the stress triaxiality is not constant during tensile deformation. This result is consistent with the findings of other scholars[30,31]. For the Lode parameter, the value for all round notched bar specimens keeps the constant of 1 during the tensile process; the value for flat grooved plate specimens drops rapidly from the initial value of approximately one at the starting point of the plastic deformation, and then stabilizes at approximately zero until fracture occurs. This is because these plate specimens were not under ideal plane strain states at the initial stage of plastic deformation, resulting in Lode parameter deviating from the theoretical value. With the increase of deformation, the specimens gradually enter the state of plane strain.

In this study the values of the stress triaxiality (η) and Lode parameter (μ_σ) are determined at the instance of failure. The relevant data about the specimens are listed in Tables 3 and 4. The tensile displacement d is the average of the two sets of tensile displacements for each kind of specimen at the

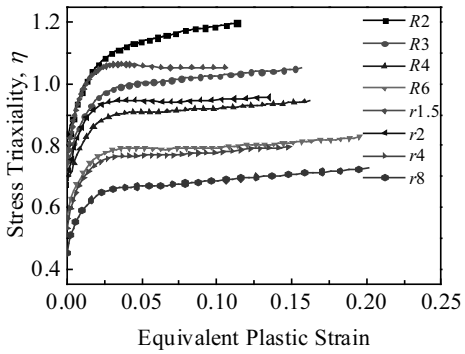

Fig.8 Curves of stress triaxiality versus equivalent plastic strain

Table 3 Relevant data of the round notched bar specimens

R/mm	η	μ_σ	d/mm	ε_f
2	1.12	1	0.467	0.04
3	1.02	1	0.533	0.082
4	0.93	1	0.615	0.123
6	0.83	1	0.808	0.195

Table 4 Relevant data of the flat grooved plate specimens

r/mm	η	μ_σ	d/mm	ε_f
1.5	1.06	0	0.383	0.045
2	0.94	0	0.396	0.080
4	0.80	0	0.49	0.150
8	0.73	0	0.608	0.202

beginning of the fracture. ε_f represents the failure strain at the center of the FE model.

The fracture loci constructed in the space of stress triaxiality and failure strain using the data listed in Tables 3 and 4 are shown in Fig.9. The failure strains of both of the round notched bar specimens and flat grooved plate specimens decrease as the stress triaxiality increases. However, different specimen configurations have different failure strains when the stress triaxialities are equal. This observation demonstrates that the failure strain is affected by the Lode parameter. The differences among the failure strains of different specimen configurations decrease as the stress triaxiality increases. This observation indicates that the influence of the Lode parameter decreases with increases in the stress triaxiality.

3 Fractography

The fracture surfaces of the specimens were studied using a JEOL JSM-7100F scanning electron microscope (SEM) to understand the ductile fracture mechanism at different stress triaxialities and Lode parameters. Additionally, the conclusions of Fig.9 could also be explained microscopically. The fractographs of the specimens were obtained from the centers of the fracture surfaces. The fractographs clearly showed that

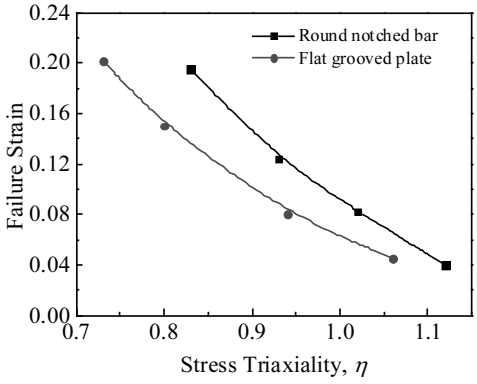

Fig.9 Fracture loci constructed in the space of stress triaxiality and failure strain

the rupture mode of both specimen configurations was void growth, which was determined by large equiaxed dimples on the fracture surface.

Representative fractographs with the same Lode parameter (μ_σ=1) but different stress triaxialities (η=0.93, 1.12) are given in Fig.10 to study the effects of the stress triaxiality. Fig.10 shows that the typical morphology of the voids did not change with the stress triaxiality changes; however, a high stress triaxiality leads to slow void growth and results in shallow dimples on the fracture surface. This finding demonstrates that the specimen with a high stress triaxiality fails in a low strain (η=1.12, ε_f=0.104; η=0.93, ε_f=0.123).

The effect of the Lode parameter could be studied by

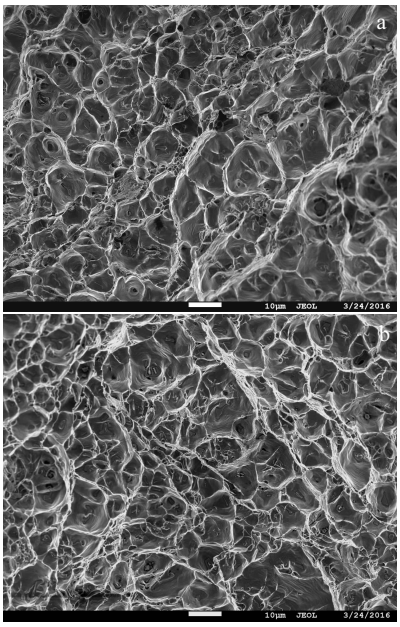

Fig.10 Representative fractographs with the same Lode parameter (μ_σ=1) but different stress triaxialities: (a) η=0.93 and (b) η=1.12

comparing the SEM images with equal triaxialities and different Lode parameters. Fractographs for round notched bar specimens, where η=0.93 and μ_σ=1, and flat grooved specimens where η=0.94 and μ_σ=0, are shown in Fig.11. The morphologies of the voids of different Lode parameters are obviously different. For the case of μ_σ=0, the dimples are few and shallow, as a sign of the low failure strain. This finding agrees well with macroscopic analysis. The nucleation rate and the growth degree of the secondary voids are also different.

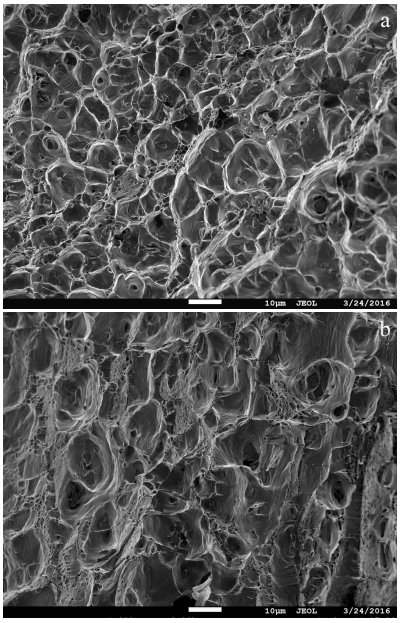

Fig.11 Fractographs with equal triaxialities but different Lode parameters: (a) η=0.93, μ_σ=1 and (b) η=0.94, μ_σ=0

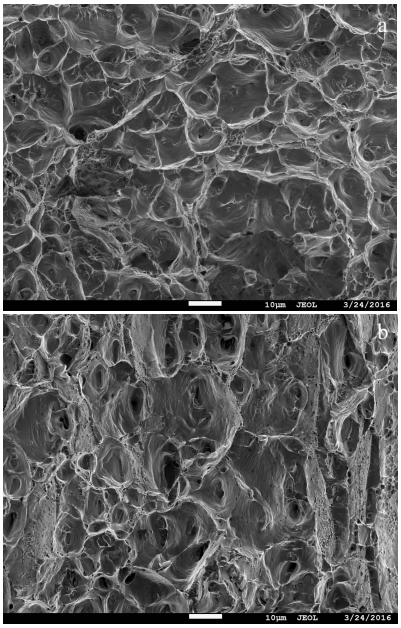

Fig.12 SEM images for the case of η=1.12, μ_σ=1 (a) and η=1.06, μ_σ=0 (b)

The SEM images for the case of η=1.12 (μ_σ=1) and η=1.06 (μ_σ=0) are shown in Fig.12. Fig.12 shows that the difference in the morphology of the two fracture surfaces is considerably smaller than that shown in Fig.11. This finding demonstrated that the effect of the Lode parameter decreases as the stress triaxiality increases.

4 Conclusions

1) The stress triaxialities of all specimens change constantly during the stretching process. The Lode parameters of flat grooved plate specimens stabilize at approximately zero before fractures occur, and the values of round notched bar specimens remain unchanged.

2) The failure strains of both specimen configurations decrease as stress triaxiality increases.

3) Large stress triaxialities lead to slow void growths and shallow dimples, which indicate that the specimen fails in a low strain.

4) The nucleation rate and the growth degree of the secondary voids are affected by the Lode parameter. When the Lode parameter is equal to zero, the dimples are few and shallow.

References

1 Guo Y Q, Zhu X F, Yang Y *et al*. *Forging & Stamping Technology*[J], 2015, 40(3): 1 (in Chinese)
2 Sun H T, Shen G Z, Hu P *et al*. *Mechanical Science and Technology for Aerospace Engineering*[J], 2010, 29(3): 379 (in Chinese)
3 Li G H, Xiong F, Long J Q. *Development and Application of Materials*[J], 2009, 24(2): 87 (in Chinese)
4 Maoût N L, Lemn T S, Manach P Y. *Engineering Fracture Mechanics*[J], 2009, 76(9): 1202
5 Zhu Z G. *Light Metals*[J], 2011, 10: 3 (in Chinese)
6 Ye T, Wang G, Yao Z G *et al*. *The Chinese Journal of Nonferrous Metals*[J], 2014, 24(4): 878 (in Chinese)
7 Liu H J, Zhang X, Xiao L F. *Journal of Machine Design*[J], 2011, 28(2): 18 (in Chinese)
8 Huang W H, Kang M, Yuan F A *et al*. *Special Casting & Nonferrous Alloys*[J], 2014, 34(7): 754 (in Chinese)
9 Xiao H D, Chai H J, Zhang J Q. *Transport Standardization*[J], 2010, 23: 41 (in Chinese)
10 Xue L, Wierzbicki T. *International Journal of Solids and Structures*[J], 2009, 46(6): 1423
11 Bai Y L. *Thesis for Doctorate*[D]. Cambridge: *Massachusetts Institute of Technology*, 2008: 26
12 Bridgman P W. *Studies in Large Plastic Flow and Fracture*[M]. New York: McGraw-Hill, 1952
13 McClintock F A. *Journal of Applied Mechanics*[J], 1968, 35(2): 363
14 Hancock J W, Mackenzie A C. *Journal of the Mechanics and Physics of Solids*[J], 1976, 24(2): 147
15 Needleman A, Tvergaard V. *Journal of the Mechanics and Physics*

of Solids[J], 1984, 32(6): 461
16 Bai Y L, Teng X Q, Wierzbicki T. *Journal of Engineering Materials and Technology*[J], 2009, 131(2): 021 002-1
17 Fouad H. *Materials & Design*[J], 2010, 31(3): 1117
18 Bao Y B, Wierzbicki T. *International Journal of Mechanical Sciences*[J], 2004, 46(1): 81
19 Wierzbicki T, Bao Y B, Lee Y W *et al*. *International Journal of Mechanical Sciences*[J], 2005, 47(4): 719
20 Barsoum I, Faleskog J. *International Journal of Solids and Structures*[J], 2007, 44(6): 1768
21 Lemaitre J, Desmorat R, Sausay M. *European Journal of Mechanics*[J], 2000, 19(2): 187
22 Ghajar R, Mirone G, Keshavarz A. *Materials & Design*[J], 2013, 43: 513
23 Kim J, Gao X, Srivatsan T S. *Engineering Fracture Mechanics*[J], 2004, 71(3): 379
24 Tvergaard V, Niordson C. *International Journal of Plasticity*[J], 2004, 20(1): 107
25 Anderson D, Winkler S, Bardelcik A *et al*. *Materials & Design*[J], 2014, 60: 198
26 Zhang K S, Bai J B, Francois D. *International Journal of Solids and Structures*[J], 2001, 38(32-33): 5847
27 Gao X S, Kim J. *International Journal of Solids and Structures*[J], 2006, 43(20): 6277
28 Joun M, Choi I, Eom J. *Computational Materials Science*[J], 2007, 41(1): 63
29 Bao Y B, Wierzbicki T. *Journal of Engineering Materials and Technology*[J], 2004, 126(4): 314
30 Brünig M, Gerke S, Schmidt M. *International Journal of Fracture*[J], 2016, 200(1-2): 63
31 Algarni M, Bai Y, Choi Y. *Engineering Fracture Mechanics*[J], 2015, 147: 140

应力三轴度和罗德参数对铝合金韧性断裂的影响

刘立熙[1,2]，郑清丽[1]，朱　健[3]，李志强[1,3,4]

(1. 太原理工大学，山西 太原 030024)

(2. 西安交通大学，陕西 西安 710049)

(3. 材料强度与结构冲击山西省重点实验室，山西 太原 030024)

(4. 北京理工大学 爆炸科学与技术国家重点实验室，北京 100081)

摘　要：大量研究表明应力三轴度对韧性断裂有重要影响。然而，最新研究表明，与应力偏张量第三不变量相关的罗德参数也是影响韧性断裂的重要因素。采用 7075 铝合金制成的缺口圆棒和凹槽平板试样分析了应力三轴度和罗德参数对韧性断裂的影响及相应的微观机理。通过准静态拉伸试验和数值模拟得到应力三轴度、罗德参数及失效轨迹，同时利用扫描电镜分析了试样不同应力状态下的空穴演化规律。结果表明，应力三轴度和罗德参数对破坏应变有重要影响，并且罗德参数的影响随应力三轴度的增加而降低。断口分析表明，孔洞的尺寸随着应力三轴度的增大而减小，不同罗德参数的空穴形态明显不同。二级孔洞的成核速率和生长程度也受罗德参数的影响。

关键词：应力三轴度；失效应变；罗德参数；断口形貌

作者简介：刘立熙，男，1990 年生，硕士，太原理工大学应用力学与生物医学工程研究所，山西 太原 030024，电话：0351-6014455，E-mail: liulixi1991@163.com